Theoretical study of the maximum power point of n-type and p-type crystalline silicon space solar cells

M A Cappelletti[1], **G A Casas**[1,2]**, A P Cédola**[1] **and E L Peltzer y Blancá**[1]

[1] Grupo de Estudio de Materiales y Dispositivos Electrónicos (GEMyDE), Dpto. de Electrotecnia, Facultad de Ingeniería, Universidad Nacional de La Plata, 48 y 116, CC.91, La Plata (1900), Argentina
[2] Universidad Nacional de Quilmes, Roque Saenz Peña 352, Bernal (1876), Buenos Aires, Argentina

E-mail: gemyde@ing.unlp.edu.ar

Abstract
The performance of crystalline silicon $n^+/p/p^+$ and $n^+/n/p^+$ solar cells under AM0 spectrum, irradiated with 1 MeV electrons at fluences below 10^{17} cm^{-2} has been analyzed by means of computer simulation. The software used, fully developed by the authors, solves numerically in one dimension under steady-state conditions, the Poisson and continuity equations self-consistently. The influence of constructive characteristics and different levels of hazardous environmental work conditions on the maximum power point of over 150 devices has been investigated. The study has allowed the authors to propose a useful analytical model related to the constructive characteristics of the device such as polarity, base resistivity and total thickness, with the aim of examining the electrical performance of Si space solar cells. Results presented in this paper are important in order to contribute to the design of radiation-hardened devices.

1. Introduction

Taking into account the urgent need to make the most of alternative energy sources, the study of semiconductor devices that can provide power at low operating cost, such as solar cells, is extremely important at the present time. Deep studies about so-called third generation solar cells, focused on new materials and technologies such as intermediate band, quantum dots and hot-carrier devices [1–4], are being carried out with the aim of reducing the cost and increasing the efficiency with respect to the first generation, i.e. crystalline silicon (c-Si) solar cells. However, in present times a considerable amount of research in the field of the photovoltaic cells is still dominated by the conventional c-Si devices.

For space power applications, where the devices are exposed to irradiation of high energy particles, multijunction (MJ) solar cells based on III–V technologies have demonstrated higher conversion efficiencies and radiation-resistance than c-Si devices [5–7]. Nevertheless, c-Si solar cells have proven to offer a worthy operational reliability and cost effectiveness as a space power source [8–10] and therefore further research in this topic is still required.

Every different solar cell structure from a given material, total thickness, base resistivity and polarity (p- or n-type), is expected to respond differently as a function of radiation. Therefore, each device must undergo some kind of irradiation test to determine the degradation characteristics. Nowadays, precise techniques of modeling and simulation have become fundamental tools to predict and to improve the response of electronic devices under different operation conditions, offering valuable knowledge at a much lower cost and in less time than experimentation.

In order to contribute to the design of radiation-hardened devices, this paper presents a theoretical study of the behavior of different c-Si $n^+/p/p^+$ and $n^+/n/p^+$ solar cells under AM0 spectrum, irradiated with 1 MeV electrons at fluences below 10^{17} cm^{-2}. Results have been obtained by using a computer program specifically designed for simulation of optoelectronic devices, fully developed by the authors. The routines solve numerically in one dimension the Poisson and continuity equations self-consistently. Simulations were carried out by varying the base resistivity and the total thickness of the cells, with the aim of understanding the influence of constructive characteristics and different levels

of hazardous environmental work conditions on the maximum power point (P_{MPP}) of the solar cells, which is the electrical parameter most strongly affected under high fluence irradiation with high energy particles including electrons and protons [11, 12]. An analytical model has been proposed and used to examine the electrical performance of Si space solar cells.

2. General remarks on the simulation code

The system of differential equations to be solved numerically, in one dimension and in steady state, consists of the coupled Poisson and continuity equations for electrons (e^-) and holes (h^+):

$$\frac{d^2V}{dx^2} = \frac{q}{\varepsilon} \cdot (n - p + N_A^- - N_D^+ + n_t - p_t)$$
$$\frac{dJ_n}{dx} = R - G(x)$$
$$\frac{dJ_p}{dx} = -(R - G(x)), \tag{1}$$

where V is the electrostatic potential, ε is the permittivity of the material, q is the electron charge, n and p are the electron and hole densities, N_D^+ and N_A^- are the shallow donor and acceptor ionized concentrations, n_t and p_t are the trapped electron and hole concentrations, and J_n and J_p represent the electron and hole current densities, respectively, which are based on the drift-diffusion (DD) model. R is the net electron–hole recombination rate including radiative, Auger, multiple deep-trap levels and impact ionization mechanisms. Recombination through multiple deep-trap levels in the bandgap is described by the Shockley–Read–Hall (SRH) theory [13, 14]. Finally, $G(x)$ is the solar-induced carrier generation rate at a distance x below the exposed semiconductor surface given by [15, 16]:

$$G(x) = \int_0^\infty G(\lambda, x) \, d\lambda = \int_{\lambda_1}^{\lambda_2} \alpha(\lambda) \cdot (1 - r(\lambda))$$
$$\cdot N(\lambda, 0) \cdot Q(\lambda) \cdot \exp[-\alpha(\lambda) \cdot x] \, d\lambda, \tag{2}$$

where λ_1 and λ_2 are, respectively, the lower and upper limits of the wavelengths of absorbed photons, $\alpha(\lambda)$ is the absorption coefficient, $r(\lambda)$ is the reflection coefficient ($1 - r(\lambda)$ is the fraction of photons that penetrates the semiconductor), $Q(\lambda)$ is the internal quantum efficiency (the average number of electron–hole pairs created by each absorbed photon, assumed equal to one in this work) and $N(\lambda, 0)$ is the incident photon flux at the surface (photons per unit area per second). Models for physical parameters such as carrier mobilities and lifetimes were extracted from [17].

In figure 1 can be seen a simplified outline of the $n^+/p/p^+$ and $n^+/n/p^+$ structures considered in this paper. L is the total thickness of the devices, and x_F, x_B and x_R are the thicknesses of front (n^+), base (p- or n-type) and rear (p^+) regions, respectively. For simulation purposes, the p^+-contact is placed at $x = 0$, whereas the n^+-contact is located at $x = L$. It has been assumed that photons and electrons penetrate the device through the n^+ layer.

Dirichlet boundary conditions for the surface potential and majority carriers (ψ_S, $n(L)$ and $p(0)$) have been fixed, assuming equilibrium with electrons in the metal and low
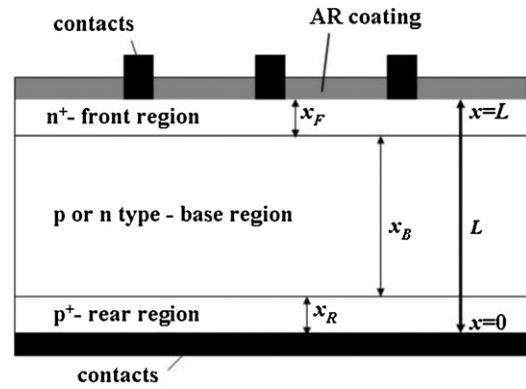

Figure 1. Schematic vertical cross section of the simulated solar cells. Reasonable thicknesses, doping profiles and physical parameters have been adopted for simulation purposes.
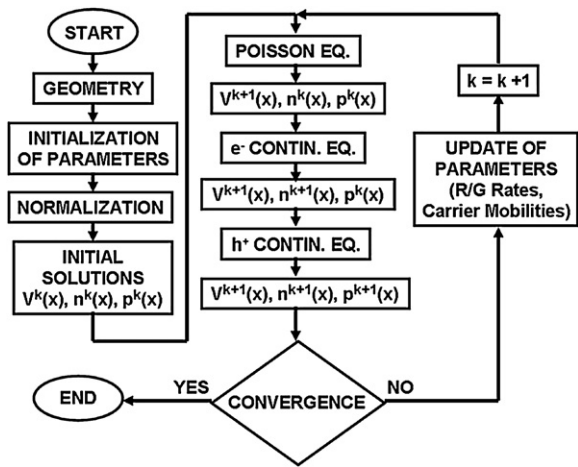

Figure 2. Flow diagram of the algorithm implemented in the software developed. Unknowns V, n and p are iteratively calculated by means of the Gummel method, in each point of the mesh.

injection level. The surface minority carriers ($n(0)$ and $p(L)$) have been calculated through current boundary condition [1]. Equations (3) and (4) correspond to the p^+- and n^+-contacts, respectively:

$$\psi_S(0) = V(0) + \frac{k \cdot T}{q} \cdot \ln\left(\frac{p_0(0)}{n_i}\right)$$
$$V(0) = 0$$
$$J_n(0) = q \cdot S_n \cdot (n(0) - n_0(0)) \tag{3}$$

$$\psi_S(L) = V(L) - \frac{k \cdot T}{q} \cdot \ln\left(\frac{n_0(L)}{n_i}\right)$$
$$V(L) = V$$
$$J_p(L) = q \cdot S_p \cdot (p(L) - p_0(L)), \tag{4}$$

where n_0 and p_0 are the electron and hole densities in thermodynamic equilibrium, S_n and S_p are effective surface recombination velocities for electrons and holes, respectively, k is the Boltzmann constant, T is the temperature and n_i is the intrinsic carrier concentration.

A flow diagram of the algorithm used in the simulation code developed is shown in figure 2. At first, a simulation

domain representing the device geometry is defined. After that, parameters related to the operating conditions and the semiconductor materials are initialized and the set of three basic semiconductor equations (1) is normalized and discretized onto variable mesh-point spacings. Discretization is carried out by means of the finite difference method, and the current densities are formulated using the Scharfetter–Gummel approach [18]. In each point of the mesh, the electrostatic potential V and the carrier concentrations n and p are iteratively calculated by means of the Gummel method [19], which is able to converge even starting from very far initial estimations with regard to the true solution. This method successively improves the unknowns V, n and p in a self-consistent way, solving for every iteration Poisson and continuity equations separately, and introducing at each step the solution at the previous one as the best approximation to the final result. Physical models such as generation/recombination rates and carrier mobilities are updated after each Gummel iteration too.

In recent years, the use of our software has allowed to successfully study the behavior of Si PIN photodiodes subject to space radiation effects [20–23].

3. Radiation damage model

The degradation of devices in the space environment is strongly dependent on the type and energy of the incident particles, properties of the semiconductor materials, and particular mission variables as orbital altitude, inclination and elapsed time after launch [24]. Under these operation conditions, the devices can suffer important radiation effects such as decrease of the minority-carrier diffusion length (minority carrier lifetime), carrier removal (including possible type conversion effects), carrier mobility degradation, multiple deep-trap levels and increase of the series resistance [25].

Most of the degradation of Si space solar cells properties after irradiation with 1 MeV electrons at fluences up to 10^{17} cm^{-2} is caused by the introduction of radiation-induced recombination centers, which reduce the minority-carrier diffusion length in the base layer of the devices. This process can be described by means of the conventional minority-carrier diffusion length degradation model, expressed by [26]:

$$\Delta(1/L^2) = (1/L_\phi^2) - (1/L_0^2) = \sum_i I_{ri} \cdot \sigma_i \cdot v \cdot \phi/D = K_L \cdot \phi,$$
(5)

where L_0 and L_ϕ are the minority-carrier diffusion length before and after irradiation, respectively, I_{ri} is the introduction rate of the ith recombination center by electron irradiation, σ_i is the capture cross section of minority carrier by ith recombination center, v is the thermal velocity of minority carrier, ϕ is the accumulated electron fluence, D is the minority-carrier diffusion coefficient and K_L is the damage constant for minority-carrier diffusion length.

However, in the range of fluences considered in this work (below 10^{17} cm^{-2}), radiation-induced defects can also cause carrier removal effect, removing majority carriers (increasing the resistivity) in the base layer. This, in turn, acts to increase the depletion region width and thereby increase

carrier collection in the base until some level where the type conversion is reached. The carrier concentration after irradiation p_ϕ in the p-Si base layer can be expressed by [26]:

$$p_\phi = p_0 \cdot \exp\left(-R_C \cdot \phi/p_0\right),$$
(6)

where p_0 is the carrier concentration before irradiation and R_C is the carrier removal rate.

Therefore, a detailed and comprehensive radiation degradation model to accurately predict Si space solar cell performance must include the combined radiation effects of K_L and R_C.

4. Simulation setup

Numerical analysis of n$^+$/p/p$^+$ and n$^+$/n/p$^+$ structures of 10×10 cm^2, with each 11 total thicknesses L, ranged from 50 to 300 μm, have been performed. In all cases, the n$^+$ and p$^+$ layer thicknesses were fixed in $x_F = 0.15$ μm and $x_R = 0.2$ μm, respectively. Different carrier concentrations varied from $N_B = 10^{14}$ to $N_B = 10^{17}$ cm^{-3} were considered for the base (p- or n-type) region of the devices simulated. Impurity densities of $N_F = 10^{19}$ and $N_R = 5 \times 10^{17}$ cm^{-3} have been used for donors in front region and for acceptors in rear region, respectively. Gaussian doping profiles were considered in all cases. Surface recombination velocities, S_n and S_p, of 2000 (passivated surface) and of 10^6 cm s^{-1} were chosen for front and rear region, respectively. An intrinsic carrier concentration at 300 K of 1.5×10^{10} cm^{-3} was used. The solar-induced carrier generation rate in silicon under one-sun, AM0 illumination at 300 K, has been obtained from (2), assuming double layer antireflective coatings (SiO$_2$/SiN). The SiO$_2$/SiN coatings have excellent antireflection properties, with less than 5% reflection in the entire wavelength range of 400–1100 nm [27, 28]. Appropriate distributions of $\alpha(\lambda)$ and $N(\lambda,0)$ were extracted from [29]. The reflection at the back of the solar cells has been neglected, being this approach a good first-approximation for the range of the total thicknesses considered in this work.

Radiation damages were studied for 1 MeV electrons, which are the main cause of solar cell degradation for Geostationary Earth Orbit (GEO). The maximum fluence considered was 10^{17} cm^{-2}. Values of K_L as a function of the base carrier concentration (p- and n-type) were obtained from [30]:

$$K_L(\text{p} - \text{Si}) = 9.7 \times 10^{-19} N_B^{0.524} \ [\text{cm}^{-3}]$$
(7)

$$K_L(\text{n} - \text{Si}) = 5.4 \times 10^{-25} N_B \ [\text{cm}^{-3}]$$
(8)

whereas $R_C = 0.15$ cm^{-1} for p-Si and $R_C = 0.3$ cm^{-1} for n-Si [30]. K_L is considered constant within the device, due to the large penetration depth of electrons in comparison with the larger thickness considered (300 μm). 1 MeV electrons impacting normally on a silicon target reach a depth of over 2000 μm, producing a practically uniform distribution of defects in the whole material [31].
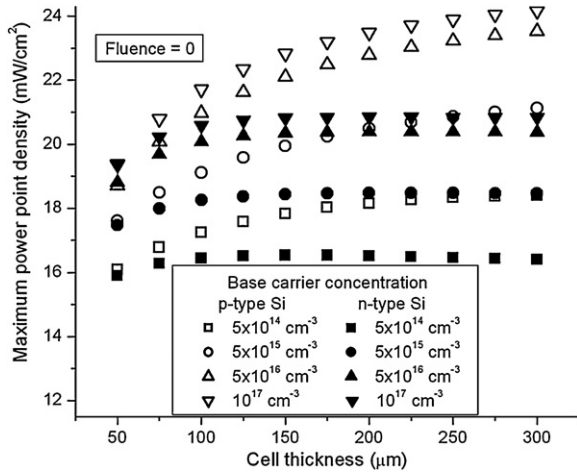
Figure 3. Increment in the maximum power point density as a function of the cell total thickness without electron irradiation. Different base carrier types and concentrations were studied.

Table 1. Maximum power point density for 16 non-irradiated solar cells with $L = 50$ μm and $L = 300$ μm and 4 different base carrier concentrations (p- and n-type).

Base carrier concentration (cm^{-3})	$P_{\text{MPP}(L = 50\ \mu m)}$ (mW cm^{-2})	$P_{\text{MPP}(L = 300\ \mu m)}$ (mW cm^{-2})	Increase (%)
5×10^{14} (p-type)	16.1	18.4	$\sim$14
5×10^{15} (p-type)	17.6	21.1	$\sim$20
5×10^{16} (p-type)	18.7	23.5	$\sim$25
10^{17} (p-type)	19.2	24.5	$\sim$27
5×10^{14} (n-type)	15.9	16.6	$\sim$4
5×10^{15} (n-type)	17.5	18.5	$\sim$6
5×10^{16} (n-type)	18.8	20.4	$\sim$8
10^{17} (n-type)	19.2	20.9	$\sim$9

5. Results and discussion

5.1. Non-irradiated solar cells subject to AM0 condition

Figure 3 shows the variation in the maximum power point density as a function of the total thickness of the devices, for different base carrier concentrations and without electron irradiation. Curves with empty symbols correspond to the n$^+$/p/p$^+$ solar cells whereas filled symbols correspond to n$^+$/n/p$^+$ devices.

A different behavior can be seen for each solar cell structure simulated. In the first place, a strong increase of P_{MPP} is observed in the entire range of L for p-type Si solar cells. By contrast, for n-type Si cells a gradual increment of P_{MPP} up to $L = 150$ μm is found, which remains unchanged between 150 and 300 μm. In turn, for $L = 50$ μm and each N_B analyzed, the P_{MPP} values are similar for the two polarities. However, when the total thickness is increased, the P_{MPP} values for the p-type Si are greater than for the n-type. This is due to the higher mobility of electrons compared to holes, by a factor of about 3, and therefore, electrons (minority carrier in p-type material) have a longer diffusion length, which leads to increase of P_{MPP}.

Table 1 summarizes the values of P_{MPP} plotted in figure 3 for minimum and maximum L analyzed in this work. Specifically, for a given base carrier concentration in the range
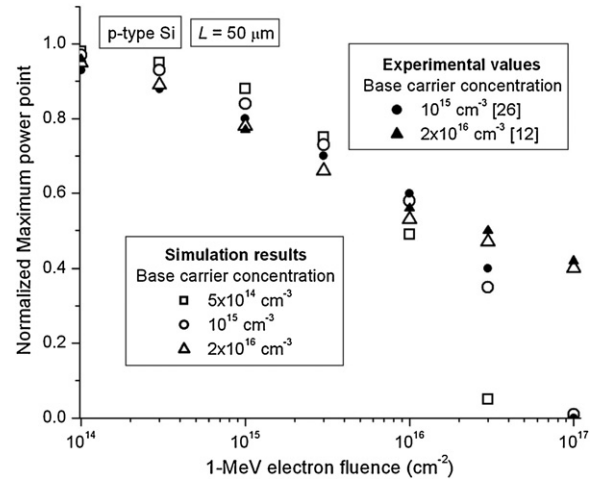

Figure 4. Degradation in the P_{MPP} of Si space solar cells as a function of 1 MeV electron fluence for a given total thickness of 50 μm. Simulation results are in agreement with experimental values.

from 5×10^{14} cm^{-3} to 10^{17} cm^{-3}, when the total thickness is increased from 50 to 300 μm, P_{MPP} values rise between 14% and 27% and between 4% and 9% for p-type and n-type Si solar cells, respectively.

The growth of the P_{MPP} with increase in the total thickness (and therefore with increase in the thickness of base x_B) is due to the fact that the incident photons have more length to travel in the thicker base region and so more region to excite trapped carriers. Then, a larger number of carriers reach the device electrodes to contribute to the generated photocurrent.

On the other hand, for a given total thickness, a change in the N_B from 5×10^{14} cm^{-3} to 10^{17} cm^{-3} produces an increment of P_{MPP} between 19% and 32% for the p-type Si and between 20% and 26% for the n-type Si approximately. This is due to the decrease of the saturation current, and therefore to the increase of the open-circuit voltage, when the base impurity concentration is increased [32].

Therefore, in all cases (p- and n-type), in the range of studied constructive characteristics, the best performance of the devices is observed when the highest base carrier concentration and total thickness are considered.

5.2. Solar cells under 1 MeV electron fluence at AM0 condition

Results on the degradation of P_{MPP} after electron irradiation are shown in figure 4, for the n$^+$/p/p$^+$ solar cell with $L = 50$ μm and three different base carrier concentrations. Curves with empty symbols correspond to simulation results whereas filled symbols correspond to experimental values [12, 26]. Values presented are normalized to those corresponding to the non-irradiated devices. It can be seen that a gradual decrease of P_{MPP} is observed for fluence irradiation below 10^{16} cm^{-2}, which can be understood by a decrease of minority-carrier diffusion length with high-energy electron [26]. For higher fluence irradiation above 10^{16} cm^{-2}, the change in P_{MPP} is different according to the base carrier concentration. An abrupt decrease in P_{MPP} is obtained when N_B is less than 10^{15} cm^{-3},
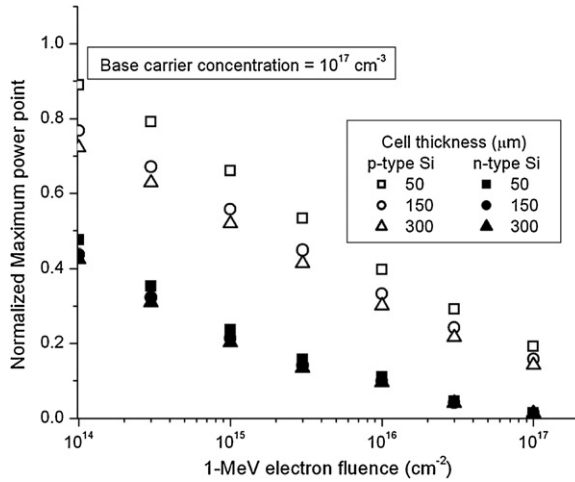
Figure 5. Degradation in the maximum power point of Si space solar cells as a function of 1 MeV electron fluence for a given base carrier concentration of 10^{17} cm^{-3}.

Figure 6. $P_{MPP}(\phi)/P_{MPP}(0)$ ratio against the cell total thickness at $\phi = 10^{15}$ cm^{-2}. Different base carrier types and concentrations were studied.

which can be attributed to the decrease in carrier concentration and increase in resistivity of the base layer. As a result of these effects, a significant increase in the series resistance of the Si solar cells is expected and the power generated by the device is dissipated by its own internal resistance, leading to severe failure of the solar cells. By contrast, when the base carrier concentration is increased by an order of magnitude ($N_B = 2 \times 10^{16}$ cm^{-3}), the carrier removal effect has almost no influence in the complete range of electron irradiation fluence considered.

Decrease of P_{MPP} as a function of 1 MeV electron fluence is shown in figure 5, for p-type and n-type Si solar cell with different total thicknesses L, from 50 to 300 μm, and $N_B = 10^{17}$ cm^{-3}. Only a few curves were plotted in this graphic for clarity. Values presented are normalized to those corresponding to the non-irradiated devices. Curves with empty symbols correspond to p-type whereas filled symbols correspond to n-type cells. It can be clearly seen that p-type are more resistant to radiation than n-type devices. For this reason, the space industry has adopted the n$^+$/p/p$^+$ solar cells for development and deployment [33]. Also, devices with smaller L are shown to have better radiation tolerance.

In order to fully understand degradation in P_{MPP} induced by high fluence 1 MeV electron irradiation for different base carrier concentrations and total cell thicknesses, it is important to consider the $P_{MPP}(\phi)/P_{MPP}(0)$ ratio, where $P_{MPP}(0)$ and $P_{MPP}(\phi)$ are the maximum power point before and after irradiation, respectively. Figure 6 shows this ratio as a function of the total cell thickness for a given electron fluence of $\phi = 10^{15}$ cm^{-2}. Different base carrier concentrations have been analyzed. Curves with empty symbols correspond to the n$^+$/p/p$^+$ solar cells whereas filled symbols correspond to n$^+$/n/p$^+$ devices.

In contrast with non-irradiated case (figure 3), the best performance of the all devices (p- and n-type) is observed when the lowest N_B and L are considered. Therefore, there is a trade-off between the base carrier concentration and the total cell thickness for improving radiation tolerance of Si space solar cells.
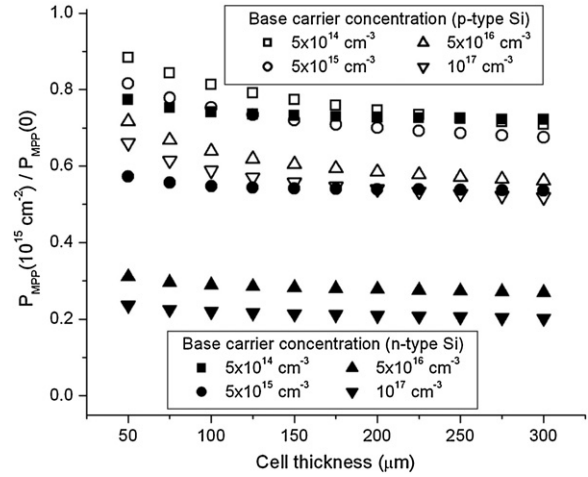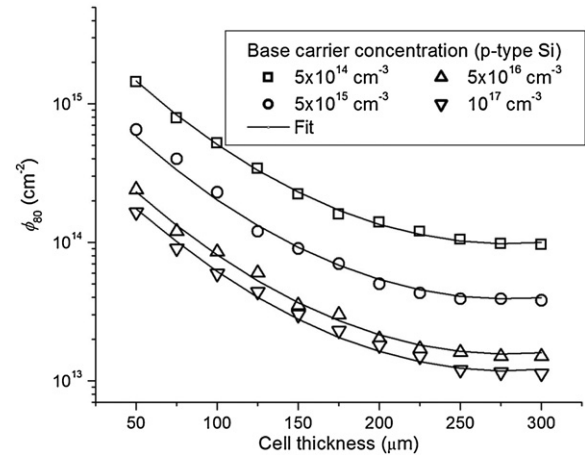

Figure 7. ϕ_{80} decay with increasing L and N_B from simulations (symbols) and fit (lines, equation (9)) for all studied p-type solar cells.

From an interpolation for each of the curves obtained in figure 5, for the entire range of L and N_B considered in this paper, the highest fluence has been calculated in order to prevent $P_{MPP}(\phi)/P_{MPP}(0)$ ratio becoming lower than 80 %. This fluence is named by the authors as ϕ_{80}. Figures 7 and 8 show the overall results obtained for p- and n-type Si solar cells, respectively.

Equation (9), found from second-order fit of curves plotted in figures 7 and 8, relates ϕ_{80} to L and N_B in p- and n-Si devices:

$$\log(\phi_{80}) = a_1 + a_2 \cdot \log(N_B) + a_3 \cdot L + a_4 \cdot L^2, \quad (9)$$

where L and N_B are expressed in μm and cm^{-3}, respectively. Table 2 contains values of constant for equation (9) for p- and n-type. Although these calculations were done for a few values of L and N_B, they span a wide range of total thicknesses and base carrier concentrations, giving a good validity to equations.

Equation (9) is useful to determine the highest electron fluence to which the electrical parameters of the solar cell (short-circuit current, open circuit voltage, maximum power point and fill factor) with well-known resistivity and total
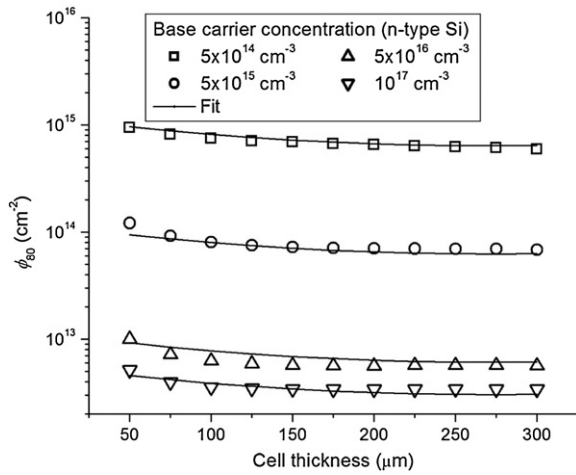
Figure 8. ϕ_{80} decay with increasing L and N_B from simulations (symbols) and fit (lines, equation (9)) for all studied n-type solar cells.

Table 2. Constant values for equation (9).

Constant	p-type	n-type
a_1	21.6	29.9
a_2	-0.4	-1.01
a_3	$-1.25 \times 10^{-2} \ \mu m^{-1}$	$-2 \times 10^{-3} \ \mu m^{-1}$
a_4	$2.23 \times 10^{-5} \ \mu m^{-2}$	$3.7 \times 10^{-6} \ \mu m^{-2}$

Table 3. Theoretical fit and comparison with experimental data.

L (μm)	N_B (cm^{-3})	ϕ_{80} (cm^{-2}) (Fit)	ϕ_{80} (cm^{-2}) (Experimental data)
50	10^{15} (p-type)	1.1×10^{15}	$\sim 1 \times 10^{15}$ (26)
100	10^{15} (p-type)	3.7×10^{14}	$\sim 4 \times 10^{14}$ (35)
100	7.2×10^{15} (p-type)	1.7×10^{14}	$\sim 2 \times 10^{14}$ (35)
250	1.5×10^{16} (p-type)	2.5×10^{13}	$\sim 4.5 \times 10^{13}$ (11)

thickness will be kept above 80% from their non-irradiated values. Additionally, the previous knowledge of the orbital location of the devices (altitude and inclination) together with the electron flux, would allow either determining the maximum exposure time or selecting the solar cell with the suitable combination of L and N_B with the aim of minimizing radiation damage.

A comparison for ϕ_{80} between equation (9) and experimental results for 1 MeV electron irradiated solar cells are presented in table 3. Value of ϕ_{80} extracted from [11] for 10 MeV proton irradiation has been converted for 1 MeV electron multiplying by 3000 [34].

For example, for a p-type Si solar cell with $L = 100 \ \mu$m, the analytical result calculated by the proposed model indicates that for an electron fluence $\phi_{80} = 3.7 \times 10^{14}$ cm^{-2}, which is equivalent to an exposure time of ten years at LEO orbit (300 km altitude, 28.5° inclination) [24], the maximum base carrier concentration is 10^{15} cm^{-3}. Under this condition, all pre-irradiation values of the device electrical parameters are reduced simultaneously in less than 20% due to 1 MeV electrons.

Although the proposed method is applied for c-Si n$^+$/p/p$^+$ and n$^+$/n/p$^+$ solar cells, it can be adapted to the analysis of MJ solar cells based on *III–V* technologies.

6. Conclusion

A computer numerical simulation tool has been developed for fast and accurate study of optoelectronic devices under different operating conditions. In particular, over 150 Si solar cells with different polarities, base resistivities and total thicknesses have been analyzed, irradiated with 1 MeV electrons at fluences below 10^{17} cm^{-2}. The results obtained have allowed us to establish trends on the electronic behavior of the space solar cells.

Non-irradiated devices subject to AM0 spectrum have been studied in the first place. In all cases, in the range of analyzed constructive characteristics, the best performance of the devices is observed when the highest base carrier concentration and total thickness are considered.

On the other hand, irradiated p- and n-type solar cells under 1 MeV electron fluence at AM0 condition have been analyzed through simulations. Results on the degradation of the maximum power point after electron irradiation have been shown in this paper. It has been found that every different solar cell structure simulated responds differently as a function of radiation. Thus, p-type devices are more resistant to radiation than the n-type. Also, unlike the non-irradiated case, devices with the smallest total thickness and base carrier concentration are shown to have better radiation tolerance. Therefore, a trade-off between the base carrier concentration and the total cell thickness for improving performance and enhancing radiation tolerance of Si space solar cells must be taken into account in order to contribute to the design of radiation-hardened devices.

Finally, from the results obtained in this study, the highest electron fluences have been found in order to prevent that the electrical parameters of the solar cell with well-known resistivity and total thickness will be degraded less than 20% from their non-irradiated values. An analytical model that relates these fluences with the constructive characteristics of the device has been proposed. Calculations done on a wide range of devices give a very general character to the derived model. This model is useful to either determine the maximum exposure time in order to avoid that the electrical parameters are degraded more than 20% from their initial values, or select the solar cell with the suitable combination of polarity, base resistivity and total thickness with the aim of minimizing radiation damage. Although the proposed model is applied for Si solar cells, it can be adapted to the analysis of MJ solar cells based on *III–V* technologies.

Acknowledgments

References

[1] Tobías I, Luque A and Martí A 2011 *Semicond. Sci. Technol.* **26** 014031

[2] Usami N *et al* 2012 *Nanotechnology* **23** 185401

[3] Guimard D *et al* 2010 *Appl. Phys. Lett.* **96** 203507

[4] Green M A 2003 *Third Generation Photovoltaics: Advanced Solar Energy Conversion* (New York: Springer)

[5] Zhang X, Hu J, Wu Y and Lu F 2010 *Semicond. Sci. Technol.* **25** 035007

[6] Guter W *et al* 2009 *Appl. Phys. Lett.* **94** 223504

[7] Green M A, Emery K, Hishikawa Y and Warta W 2009 *Prog. Photovolt. Res. Appl.* **17** 85

[8] Lee J J *et al* 2008 *J. Astron. Space Sci.* **25** 435–44

[9] Yamaguchi M 2001 *Sol. Energy Mater. Sol. Cells* **68** 31–53

[10] Khan A *et al* 2000 *Semicond. Sci. Technol.* **15** 403–7

[11] Alurralde M *et al* 2004 *Sol. Energy Mater. Sol. Cells* **82** 531–42

[12] Khan A *et al* 2003 *Sol. Energy Mater. Sol. Cells* **75** 271–6

[13] Shockley W and Read W T 1952 *Phys. Rev.* **87** 835–42

[14] Hall R N 1952 *Phys. Rev.* **87** 387

[15] Möller J 1993 *Semicond. Sol. Cells* (London: Artech House Publishers)

[16] Zhao J and Green M A 1991 *IEEE Trans. Electron Devices* **38** 1925–34

[17] Selberherr S 1984 *Analysis and Simulation of Semiconductor Devices* (New York: Springer)

[18] Scharfetter D L and Gummel H K 1969 *IEEE Trans. Electron Devices* **16** 64–77

[19] Gummel H K 1964 *IEEE Trans. Electron Devices* **11** 455–65

[20] Cappelletti M A, Urcola U and Peltzer y Blancá E L 2006 *Semicond. Sci. Technol.* **21** 346–51

[21] Cappelletti M A, Cédola A P and Peltzer y Blancá E L 2008 *Semicond. Sci. Technol.* **23** 025007

[22] Cappelletti M A, Cédola A P and Peltzer y Blancá E L 2009 *Semicond. Sci.Technol.* **24** 105023

[23] Cédola A P, Cappelletti M A, Casas G and Peltzer y Blancá E L 2011 *Nucl. Instrum. Methods Phys. Res.* A **629** 392–5

[24] Stassinopoulos E G and Raymond J P 1988 *Proc. IEEE* **76** 1423–42

[25] Leroy C and Rancoita P G 2007 *Rep. Prog. Phys.* **70** 493–625

[26] Yamaguchi M *et al* 1996 *Appl. Phys. Lett.* **68** 3141

[27] Chen Z, Sana P, Salami J and Rohatgi A 1993 *IEEE Trans. Electron Devices* **40** 1161–5

[28] Wright D N, Marstein E S and Holt A 2005 *Proc. 31st IEEE Photovoltaic Specialists Conf. (Florida)* pp 1237–40

[29] Sze S M and Ng K K 2007 *Physics of Semiconductor Devices* 3rd edn (New York: Wiley)

[30] Yamaguchi M *et al* 1999 *IEEE Trans. Electron Devices* **46** 2133–8

[31] Spieler H 1998 *Lecture Notes-Physics 198, Spring Semester-UC* (Berkeley) (http://www-physics.lbl.gov/˜spieler/physics_198_notes/)

[32] Goetzberger A, Knobloch J and Voss B 1998 *Crystalline Silicon Solar Cells* (New York: Wiley)

[33] Cotter J E *et al* 2006 *IEEE Trans. Electron Devices* **53** 1893–901

[34] Yamaguchi M *et al* 1996 *J. Appl. Phys.* **80** 4916–20

[35] Suzuki A 1998 *Sol. Energy Mater. Sol. Cells* **50** 289–303